JGR Atmospheres

RESEARCH ARTICLE
10.1029/2021JD035350

The Character and Changing Frequency of Extreme California Fire Weather

Andreas F. Prein[1], Janice Coen[1,2], and Abby Jaye[1]

[1]National Center for Atmospheric Research (NCAR), Boulder, CO, USA, [2]University of San Francisco, San Francisco, CA, USA

Key Points:

- Fire weather types (WTs) are shown to be related to the largest burned area days in recent decades in eight Californian regions
- Increases in Diablo and Santa Ana WT events during the 20th century are primarily caused by natural climate variability
- Changing greenhouse gas and aerosol forcing significantly increase thermal-low WTs in coastal regions and the western Sierra

Supporting Information:

Supporting Information may be found in the online version of this article.

Correspondence to:

A. F. Prein,
prein@ucar.edu

Citation:

Prein, A. F., Coen, J., & Jaye, A. (2022). The character and changing frequency of extreme California fire weather. *Journal of Geophysical Research: Atmospheres*, *127*, e2021JD035350. https://doi.org/10.1029/2021JD035350

Received 1 JUN 2021
Accepted 20 APR 2022

Author Contributions:

Conceptualization: Andreas F. Prein
Data curation: Andreas F. Prein, Janice Coen, Abby Jaye
Formal analysis: Andreas F. Prein
Funding acquisition: Janice Coen
Investigation: Andreas F. Prein
Methodology: Andreas F. Prein
Project Administration: Janice Coen
Resources: Andreas F. Prein, Abby Jaye
Software: Andreas F. Prein
Supervision: Janice Coen
Validation: Andreas F. Prein
Visualization: Andreas F. Prein
Writing – original draft: Andreas F. Prein
Writing – review & editing: Andreas F. Prein, Janice Coen

Abstract Five of California's 10 largest wildfires occurred in 2020, with the largest complex exceeding the previous largest by more than 100%. The year follows a decade containing extraordinary fire activity. Previous trend investigations focused on changes in human activities and atmospheric thermodynamics, while the impacts of changing atmospheric dynamics are largely unknown. Here, we identify weather types (WTs) associated with historically large daily burned areas in eight Californian regions. These WTs characterize dominant fire weather regimes varying in fire behavior types (plume-driven vs. wind-driven fires) and seasonality. Most of the strongly large-scale forced WTs such as Santa Ana and Diablo events increased in frequency during the 20th century particularly in the San Diego and Bay Area regions. These changes are likely not anthropogenically caused and the frequency of such events is projected to decrease under continuing climate change. However, significant future increases are found for WTs associated with thermal-low-pressure systems along the California coast and in the Sierra west region. These increases in southern California are mainly due to increasing greenhouse-gas forcing and arise from the larger ocean-land temperature gradient while aerosol forcing changes are driving most of the increased frequency in central and northern California due to a reduction of relative humidity over land and a strengthening of low-pressure anomalies over the coast. These WT frequency changes could permit more weather favorable for large fire growth in summer and less in fall, further enhancing the risk of catastrophic fires due to hotter and drier summers in future climates.

1. Introduction

Among U.S. states, California has the highest exposure to wildfires, with approximately 2,019,800 properties at risk (Verisk, 2020). The combination of increasing annually burned area (Abatzoglou & Williams, 2016; Westerling, 2016) and large exposure resulted in exceptional economic losses with more than 20US$ bn in 2018 alone (Munich-Re, 2019). Potential causes for the large increase in burned area in California (FIRE, 2020) are manifold (Jin et al., 2014) and include an increase in atmospheric temperature and aridity caused by climate variability and change (Abatzoglou & Williams, 2016; Williams et al., 2019), a decrease of precipitation in recent decades due to fewer winter storms (Prein et al., 2016), an earlier start and later end of the fire season (Jolly et al., 2015), changes in forest management (Parks et al., 2015; Tempel et al., 2014), an increase in population (Radeloff et al., 2018), and its expansion of dwellings and infrastructure into former wildlands (Hammer et al., 2007). Since the early 2000s, sub-daily observations of active fires from satellites have enabled products that estimate daily burned area on local scales (Artés et al., 2019; Davies et al., 2019), revolutionizing our ability to detect fire occurrence and progression. These observations allow us to analyze the impacts of weather on fire growth and confirm that the annual total burned area in California is disproportionately affected by a few large fires and those fires themselves burn most of the total burned area in only a few days.

Traditionally, fire weather indexes—for example, Fosberg Fire Weather Index (Fosberg, 1978; Goodrick, 2002) or the Hot/Dry/Windy Index (Srock et al., 2018)—are used to predict days with the potential for rapid-fire-spread. Those indices typically depend on local observations that account for atmospheric static stability and humidity profile in the lower atmosphere (Haines, 1989), fuel condition (Amiro et al., 2005), and low-level wind speed (Amiro et al., 2005). More recent studies also found that upper-level and nocturnal meteorology can lead to rapid-fire-spread (Huang et al., 2009; Nimchuk, 1983; Peterson et al., 2015; Smith et al., 2018). However, state-of-the-art climate models have large biases in simulating local scale fire weather conditions, making it difficult to study climate change impacts on future fire weather.

We focus on the synoptic-scale atmospheric conditions that were present during days of large daily fire growth in California's recent history. These synoptic-scale conditions are more reliable simulated in current climate models than local-scale phenomenon. We hypothesize that there is a limited set of weather types (WTs) that favor large daily fire growth, which is based on research preformed in the early and mid-20th century (Potter, 2012a).

The idea of using synoptic patterns to improve fire behavior and fire danger assessments was first proposed in the early-20th century focused for fire danger in the U.S. (Beals, 1914; Joy, 1923; McCarthy, 1923) and was later applied to other fire prone regions around the world such as Australia (Foley, 1947), and Canada (Newark, 1975). Schroeder et al. (1964) performed a landmark analysis for the Contiguous United States (CONUS) by using the fire load index, which incorporates various weather variables into a fire danger index, during the period 1951–1960. Based on this index, they selected the most dangerous fire days and classified them in 14 regions over the CONUS. They separated California into Southern California and Northern and Central California. Four synoptic patterns were identified that cause the highest fire danger in the Southern California region, which are Subtropical High Aloft, Meridional Ridge-Southwest Flow, Pacific High-Post-frontal Type, and Santa Ana (i.e., Great Basin High) type. Similar types were identified for the Northern and Central California region. The Subtropical High occurs in the warmest season of the year and produces heat waves. Winds are typically weak but the atmosphere can be unstable. The southwesterly flow with a meridional ridge causes strong winds in higher elevated regions. The post-frontal type can result in high fire risk when the flow is coming from the northeast causing down-slope winds that adiabatically warm. An east to west pressure gradient is present during Great Basin High conditions resulting in Santa Ana winds in Southern California and Diablo/Mono winds in the center of the state. Hull et al. (1966) built on the work of Schroeder et al. (1964) and analyzed the frequency of critical fire weather patterns for each region with the aim to improve fire weather forecast.

More recent research mostly focuses on the three-dimensional multi-scale interaction of synoptic scale weather, mesoscale dynamics (e.g., mountain waves), and fire behavior and interested readers can find a review of this topic in Potter (2012a, 2012b).

Here, we update the techniques used, and expand on the detail provided by Schroeder et al. (1964) by using an objective data-driven method to define archetypal fire WTs and understand potential changes in their frequency under climate change. Therefore, we use daily burned area observations, state-of-the-art atmospheric reanalysis data sets, and large ensemble (LENS) climate model output.

2. Data and Methods

2.1. Fire Observations and Fire Regions

To understand how extreme fires evolve temporally, we employed daily burned area estimates based on satellite active fire-detection data collected from the Global Wildfire Information System (GWIS) data set (Artés et al., 2019). GWIS has global coverage between January 2001 and November 2019. It is primarily based on satellite observations from the MODIS burnt area product Collection 6 (MCD64A1) and applies a data mining workflow to create a global database of individual fires that characterizes fires by type and fire regime.

Our analysis is performed on eight “homogeneous” fire regions that feature similar fuel and fire weather conditions (Figure 1a). These regions are similar to the regions defined in California's Fourth Climate Change Assessment (Bedsworth et al., 2018) except that we have split the Sierra Nevada region into east and west parts to account for their different fire weather conditions. No WTs were derived for the Central Valley and the Desert Southwest due to their small sample size of observed fires. The Northern and Sierra regions are mainly forested while the central and southern coastal regions feature chaparral, grass-oak savanna, and urban areas. Also, fire ignition varies among regions and is mostly human-caused in urbanized regions, caused by dry lightning in the Northern and Modoc regions, and of mixed natural and human-caused ignitions in the Sierra regions (Balch et al., 2017).

2.2. Atmospheric Variables

The WT analysis was performed by using daily average (daily minimum and maximum for 2 m temperature) atmospheric fields from the European Centre for Medium-Range Weather Forecasts (ECMWF) fifth generation global reanalysis (ERA5; Hersbach et al., 2020) over the GWIS data record. ERA5 assimilates a large variety of

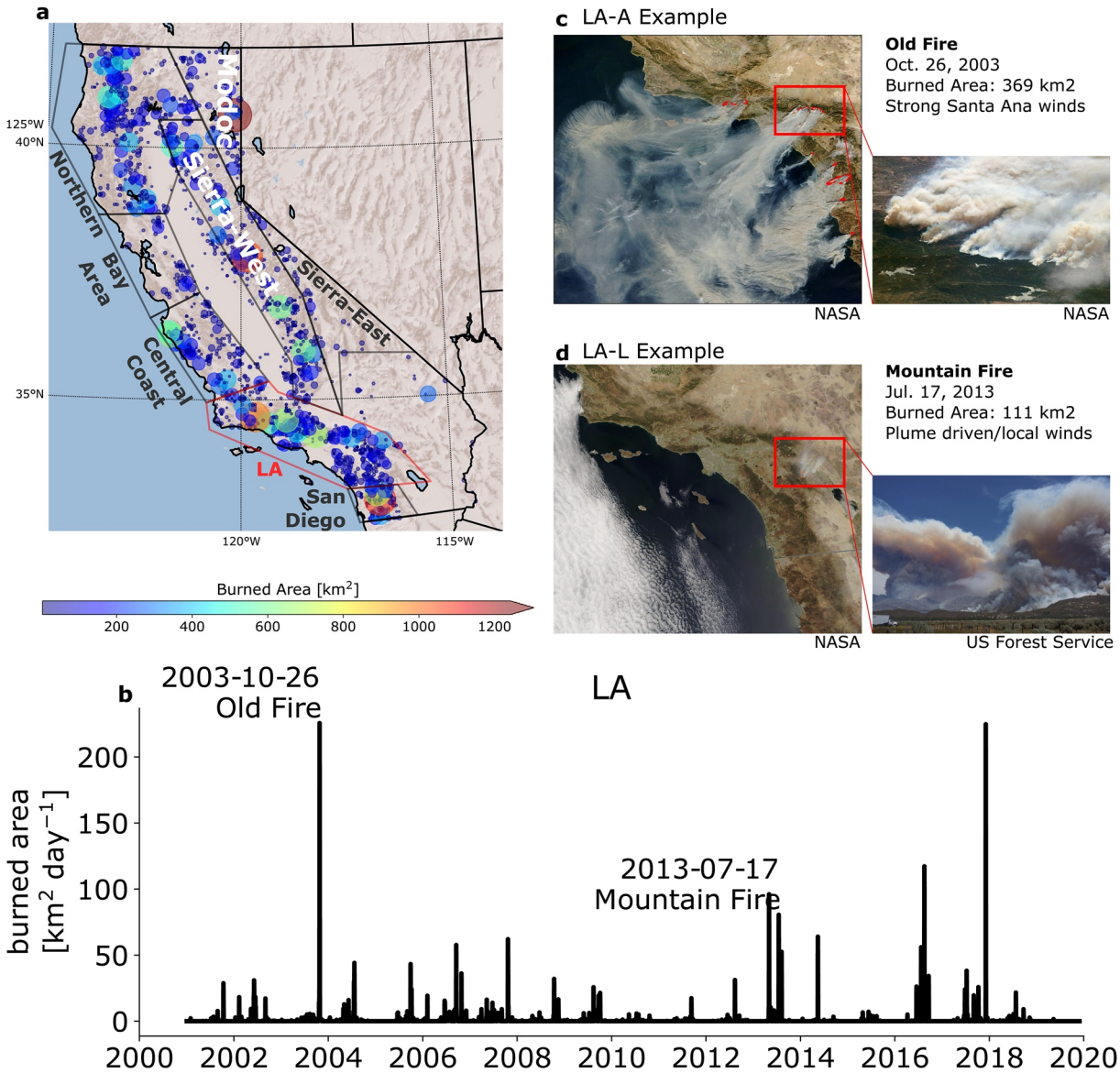

Figure 1. California fire regions and accumulated burned area (indicated by circle size and color) of fires from the Monitoring Trends in Burn Severity (MTBS) (Eidenshink et al., 2007) data sets covering 1984–2016 (a). The accumulated daily burned area time series for the LA region (highlighted in red outline in panel (a)) based on the GWIS data set is shown in (b). Images of a typical wind-driven fire ((c); Old Fire) and plume-driven fire ((d); Mountain Fire) are shown to exemplify the importance of meteorological conditions on fire behavior.

observational data including satellite, surface-based, and airborne data. We tested 31 variables concerning their suitability to identify days with extremely large burned areas (Table 1). These variables were selected due to their relevance in prescribing the synoptic-scale flow conditions and their impact on fire behavior (Amiro et al., 2005; Haines, 1989; Van Wagner, 1974).

To analyze historic and projected future changes in WT frequencies in each of the eight California fire regions we detect WT days in four data sets. First, we use the ECMWF 20th century reanalysis (ERA20C; Poli et al., 2016) which provides data from 1900 to 2010 at a grid spacing of approximately 125 km (spectral truncation T159).

Second, we use the third version of the NOAA-CIRES-DOE 20th Century Reanalysis (NCD20C; Slivinski et al., 2019). NCD20C is a probabilistic reanalysis product with 80-ensemble-members that allow the statistical analysis of WT trends within the period 1900–2015. It has an effective resolution of 60 km at the equator, assimilates a large set of pressure observations, and is forced by pre-described sea surface temperature and sea ice fields.

Table 1
Variables Used in the Weather Typing Analysis

Type of variable	Variable	Acronym [unit]	Level
Dynamic	Zonal windspeed	U [m/s]	10 m,
	Meridional windspeed	V [m/s]	850 hPa
			500 hPa
	Total windspeed	W [m/s]	200 hPa
	Geopotential height	Z [m]	500 hPa
	Sea level pressure	SLPAVG [hPa]	Sea level
Thermodynamic	Daily mean air temperature	T [°C]	2 m
			850 hPa
			500 hPa
	Daily min. air temperature	T2MIN [°C]	2 m
	Daily max. air temperature	T2MAX [°C]	2 m
Moisture	Mixing ratio	MR [g/kg]	2 m
	Relative humidity	RH [%]	850 hPa
	Moisture flux	MF [g m/kg s]	500 hPa
	Precipitable water	PWAVG [mm]	Integral
Convective[a]	Level of free convection	LFC [m]	Above
	Lifting condensation level	LCL [m]	Surface

[a]Convective variables are calculated by using the most unstable parcel, where the parcel temperature and moisture are the averages over a 500 m deep layer.

It has a largely improved representation of storm intensity, more accurate estimates of confidence intervals, reduced errors, and large-scale reductions in model biases than previous versions.

Third, we analyze the Community Earth System Model (CESM) LENS data set (Kay et al., 2015) to understand the impact of natural variability and forced climate change on WT frequencies. LENS consists of 40-ensemble members that are identical except for chaotic perturbation of the initial condition temperatures. The model grid spacing is 1° and each member covers the period 1920–2100. Historic forcing is applied to the period 1920–2005 and representative concentration pathway 8.5 (RCP8.5) forcing was used from 2006 to 2100 (Lamarque et al., 2011; Meinshausen et al., 2011).

The fourth data set that we use in the WT frequency change analysis is the CESM single forcing runs (SFR; Deser et al., 2020). These simulations are identical to the LENS simulations except for one forcing agent being held constant at its 1920 level. We are using the fixed greenhouse gas (no-GHG) and fixed aerosol (no-AER) ensembles in this study. Each of them consists of 20-members that vary in slight temperature perturbations in 1920 and provide data until 2080. The effect of greenhouse gases on WT frequencies is derived from the difference between the SFR with constant greenhouse gases and the full forcing (LENS) simulations. The same is done to derive the effect of aerosol forcing changes.

2.3. Fire WT Analysis

The process of deriving WTs for each of the eight California fire regions is shown in Figure 2. First, we load the 31 ERA5 atmospheric variables in a region that is 15° larger than the edges of the region of interest (black box in Figure 2-1) within the GWIS period (January 2001 to November 2019). We tested different box sizes for the weather typing ranging from adding 5° to 20° around the focus region. We found little sensitivity to the domain size but overall a good performance for using a weather typing domain that is 15° larger than the focus region (not shown). Second, variables are pre-processed by calculating daily relative anomalies compared to the variable's climatology and by normalizing the daily fields (mean is zero and standard deviation is one) to give the variables equal weight. Using relative anomaly fields help to assign equal weights to variables that vary greatly access the weather typing region and improves the weather typing skill (e.g., 2 m above ground mixing ratio). The WT results allow us to differentiate between changes in the synoptic-scale dynamics (e.g., the frequency of an extreme pattern) and changes in its thermodynamics (e.g., the temperature on extreme fire days).

Third, we read the GWIS daily burned area product and accumulate the daily burned area in each of the eight fire regions and select the top K events that are at least 7 days apart. We select 7 days to sample independent weather situations since this is the duration when the drop in the auto-correlation function of minimum Manhattan distances flattens in all regions (not shown). The presented results are largely insensitive to varying this value between four to 10 days. The pre-processed atmospheric variables in the analysis region (15° larger than region of interest) are selected for the top K days. We optimize the cluster analysis by testing all possible combinations of up to three variables out of the 31 variables (Table 1; 4,991 possible combinations). Previous analysis has shown that using three or fewer variables results in close to optimum clustering performance and also substantially reduces the necessary computational costs (Prein & Mearns, 2021). The selected atmospheric variables are clustered by using the output of the Ward's minimum variance hierarchical clustering method as the seed for a K-means cluster algorithm (Wilks, 2011). The combination of these two methods is highly skillful in identifying weather patterns (Schiemann & Frei, 2010). We determine the number of clusters by using the elbow method, which identifies the clustering step where the acceleration of distance growth is the biggest. In addition to the hierarchical and K-means clustering, we also tested a hierarchical density-based clustering (McInnes et al., 2017) method, which resulted in comparable skill but produced a large number of WTs for each region, which made it difficult to work with its output.

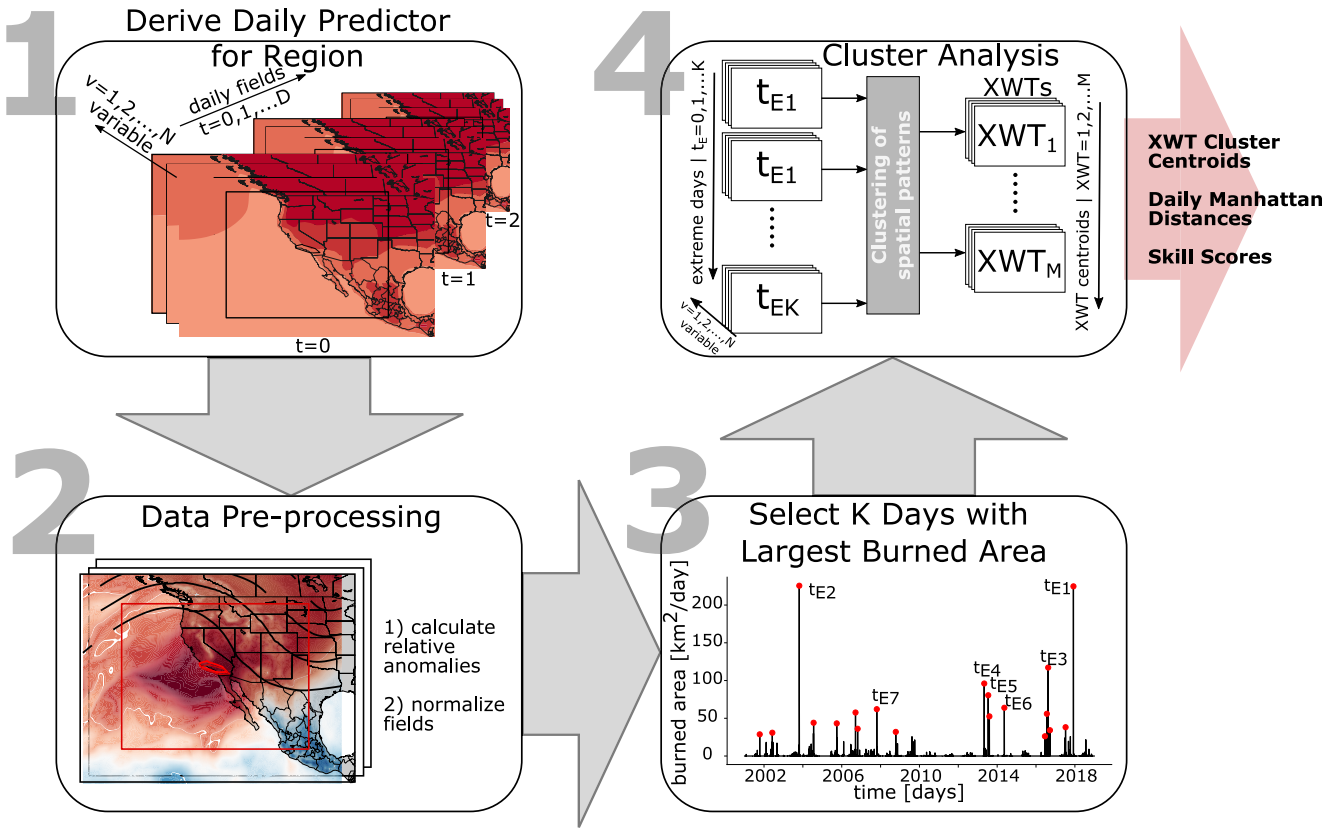

Figure 2. Flow chart of WT methodology. (a) Daily predictor variables are read for a region (black rectangle) that is 15° larger than the fire region of interest (black polygon showing the Los Angeles region). For each day, up to N predictor variables out of the 31 variables (v) are read (we use $N = 3$ resulting in 4,991 possible combinations) within the analysis period 1 January 2001 to 30 November 2019. (b) The daily predictor variables are pre-processed by calculating relative climatological anomalies and by spatially normalizing their daily anomaly patterns (each daily predictor variable has a mean of zero and a standard deviation of one). (c) The accumulated daily burned area within the target region is loaded and K days with the largest burned area that are at least 7 days apart are selected. We use $K = 19$, which results in selecting one event per year on average (i.e., annual event due to the 19 yr long observational record). (d) The predictors of the 19 extreme fire weather days are selected and used in a hierarchical and k-means cluster analysis resulting in M WTs. The output of the clustering is WT centroids, Manhattan distances for each day within the analysis period, and skill scores to evaluate the performance of the WTs in detecting days with large fire growth.

A summary of this analysis and the selected variable combinations that resulted in optimal skill in each region is shown in Figure 3. The variables that result in the highest predictive skill are mostly related to low-level moisture and temperature patterns, which agrees well with previous studies that identified hot-dry conditions as most favorable for wildfires in California (Dong et al., 2021). Additionally, 500 hPa geopotential height is also a good predictor in many regions. The lifting condensation level pattern is particularly important in the Modoc, Sierra East, and Sierra West region.

The skill of the WTs in identifying large fire growth days is calculated from a split-sample analysis where WTs are derived based on one half of the data period and their skill is evaluated compared to the other half. WTs are skillful if they allow identifying extreme fire days based on their similarity (Manhattan Distance) to a WT centroid (mean state). We use the Manhattan Distance due to its benefits for high-dimensional applications (Aggarwal et al., 2001). We also tested the Euclidean Distance, which results in similar skill scores, and the Mahalanobis Distance, which resulted in errors for variables that contain many zeros (e.g., CAPE, CIN) due to singular covariance matrices.

Several skill scores were tested and we decided to use the average of two scores that target different error characteristics. The first score is the "area under the Receiver operating characteristics (ROC) curve" (AUC; Wilks, 2011) skill score. The ROC curve is based on two parameters at different classification thresholds—the False Positive Rate (the ratio of false positives to false positives and true negatives) and the True Positive Rate

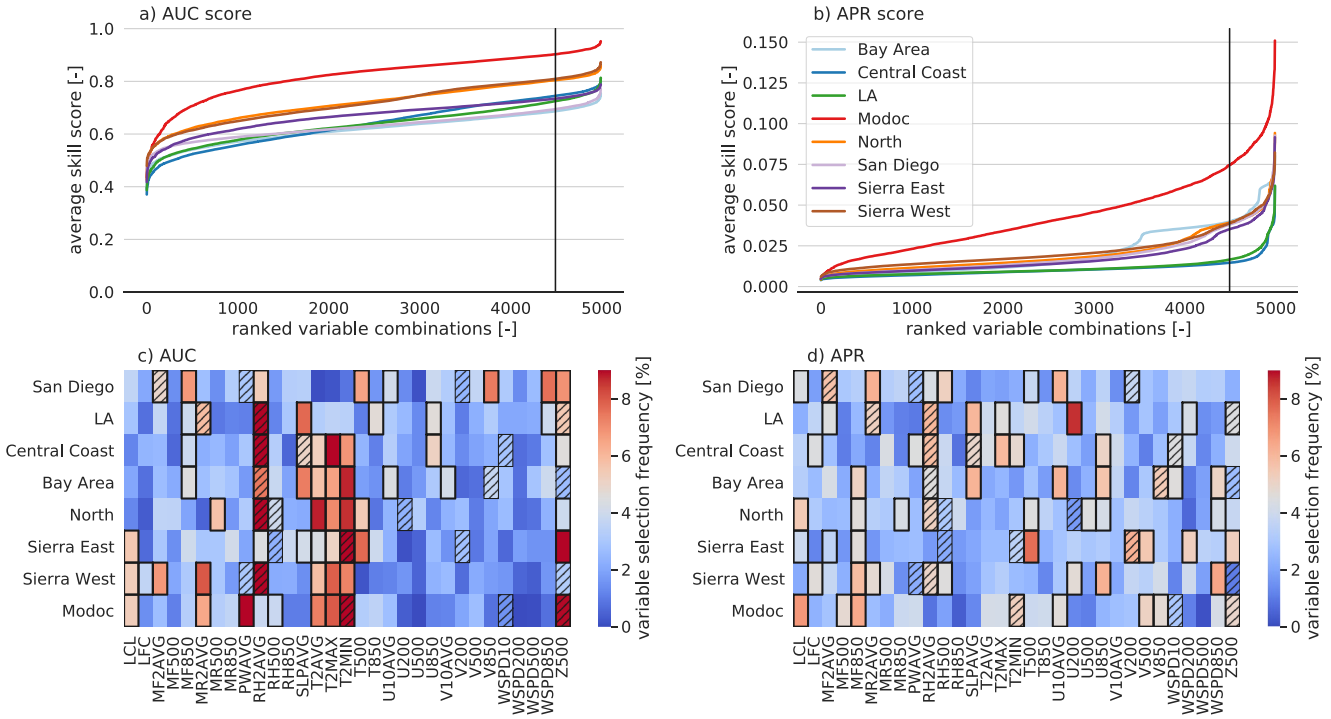

Figure 3. Average split sample AUC (a) and APR (b) skill score of all 4,991 tested variable combinations ranked from lowest to highest (one is perfect). The black vertical line shows the 10% of the best performing combinations. Probability frequency heatmap showing how often a variable was selected in the top 10% of the best performing variable combinations considering the AUC (c) and APR (d) score. The eight variables that were selected most frequently in the top performing settings are highlighted in black boxes. The three variables that are selected to define the final WT are hatched. The variables are described in Table 1.

(the ratio of true positive to true positive and false negative). The AUC is the integral under the ROC curve where a value of 1.0 indicates a perfect model and a value of 0.5 indicates a model with no skill.

The second score is the Average Precision-Recall score (Saito & Rehmsmeier, 2015; APR). Similar to the AUC this score consists of two variables— precision and recall. Precision is defined as the ratio between true positive to true positive plus false positive and recall measures the ratio between true positive to true positive and false negatives. The APR is the integral under the precision-recall curve and varies between 0.0 and 1.0, where 1.0 indicates a perfect model.

We use the Python sklearn (Buitinck et al., 2013; Pedregosa et al., 2011) package to calculate AUC and APR scores. We input a binary array as observations that is zero for all days except for the 19 days with the largest observed daily burned area, where it is one. As predictors, we calculate daily Manhattan distances to each identified WT and derive the minimum distance (i.e., the distance to the WT that the day is most similar to). Next, we normalize the daily minimum Manhattan distances to range from one (highest probability to be a WT day) to zero (lowest probability to be a WT day). This normalized array is used as the predictor in the skill score calculation.

3. Results

3.1. Fire WTs

Daily time series of burned areas are characterized by a clear seasonal cycle with summer and autumn maxima as shown for southern California by Jin et al. (2015) and feature distinct peak events such as shown in the example of the Los Angeles (LA) region in Figure 1b. Extreme fire days dominate the statistics of total burned area with the top 1% of days accounting for between 35% in the Northern region and 77% in the San Diego region. The rapid increase and decay of daily burned areas indicate that extreme fire days are closely related to short-term weather conditions more so than slowly changing factors, as found in other locations (Abatzoglou & Kolden, 2011; Riley et al., 2013).

Figure 4 shows the identified WTs of the eight fire regions. San Diego, Los Angeles, and the Bay Area region have a pattern that Schroeder et al. (1964) called Great Basin High and that we refer to as Santa Ana (A) in San Diego and Los Angeles and Diabolo (D) in the Bay Area. This pattern is associated with an east to west pressure gradient that results in strong, very dry winds from the northeast. These WTs occur most frequently between September and November and have a secondary peak in May and June. This seasonality is consistent with Santa Ana related fires in Jin et al. (2014) but differs from other studies that found a peak in Santa Ana events in December and January (Guzman-Morales et al., 2016). These differences are likely due to the methodology that is used to identify Santa Ana events. Guzman-Morales et al. (2016), for instance, use a local definition of Santa Ana events according to the wind direction and speed in California while we use large-scale moisture and pressure pattern that were present on large fire days, which also accounts for antecedent and non-local conditions in addition to weather settings.

Our algorithm split up the subtropical high WT from Schroeder et al. (1964) into multiple sub-types. The San Diego and Central Coast convective pattern (C; Figure 4c), the San Diego, Los Angeles, Central Coast, Bay Area, and Sierra West thermal low (L; Figures 4e, 4h, 4l, and 4x), the Modoc ridge in the west (R_W; Figure 4r), and the Modoc and Sierra East high (H; Figure 4w). All of these patterns most frequently occur during in summer. The thermal low pattern is associated with large burned areas in all coastal regions (except the Northern region) and in the Sierra West. It is characterized by a weak cyclonic flow that develops due to the differential heating of the lower troposphere over land and the subsequent divergence of air aloft caused by the lifting of isobaric surfaces. Thermal lows can be embedded in thermal surface troughs (see Figure 4b for an example) but are non-frontal.

The meridional ridge-southwest flow type (Schroeder et al., 1964) is characterized by a trough west of the region of interest (T_W). This pattern causes rapid fire growth in the Northern (N-T_W; Figure 4n), Modoc (M-T_W; Figure 4q), Sierra East (SE-T_W; Figure 4s), and Sierra West region (SW-T_W; Figure 4w). This WT occurs most frequently in mid-to late-summer.

The Pacific high, post-frontal type (Schroeder et al., 1964) is most prominent in the Northern region (N-T_E; Figure 4m), however, the Diablo pattern in the Sierra West region (SW-D; Figure 4v) has a similar morphology. These patterns are most frequent in fall but can also occur in spring.

Some regions have an additional WT that is different from those described in Schroeder et al. (1964). It is unknown if these additional WTs did not cause hazardous fire weather in the weather record analyzed by Schroeder et al. (1964), if they did not occur during the analyzed time period, or if they were not detected by the method used in Schroeder et al. (1964). The Bay Area experiences a pattern with strong zonal flow (BA-Z; Figure 4k) and the Northern and Modoc regions have a WT with north-easterly flow due to ridging over the east Pacific (N-R_W; Figures 4o and 4r). The Los Angeles and Sierra East regions have a third cluster that we do not identify as a WT due to their infrequent occurrence and relatively smaller burned areas (Table 2).

From Figure 4, it is obvious that some WTs can affect multiple regions such as the Santa Ana weather pattern in San Diego and Los Angeles. To understand if the WTs from one region could be used to identify large fire growth days in another region we performed a cross valuation and calculate the AUC and APR scores (Figure 5). While the AUC values can be similar among regions (e.g., using LA WTs in Modoc) the APR values are often much smaller due to the larger sensitivity of APR scores to false alarms. This analysis particularly highlights the dissimilarities between WTs in southern California (San Diego and Los Angeles) and northern California (North, Modoc, and the Sierra regions).

3.2. Representation of Fire WTs in Reanalysis and Climate Model Output

To understand how well 20th century reanalyses and the CESM model can simulate fire WTs, we identify WT days in the ERA20C, 80-member NOAA-CIRES-DOE 20th Century Reanalysis (NCD20C; Slivinski et al., 2019), the 40-member CESM LENS Kay et al., 2015), and the CESM single forcing 20-member ensemble (SFE; Deser et al., 2020). WT days are identified by regridding the WT centroids from the ERA5 to the ERA20C, NCD20C, LENS, and SFE grid pre-processing the daily predictor variables, and calculating Manhattan distances for each region and WT.

A comparison of the minimum normalized (according to grid cells and variables) Manhattan distances (minimum over the WTs in each region) among ERA5, ERA20C, and NCD20C for the common period of 2001–2010 is

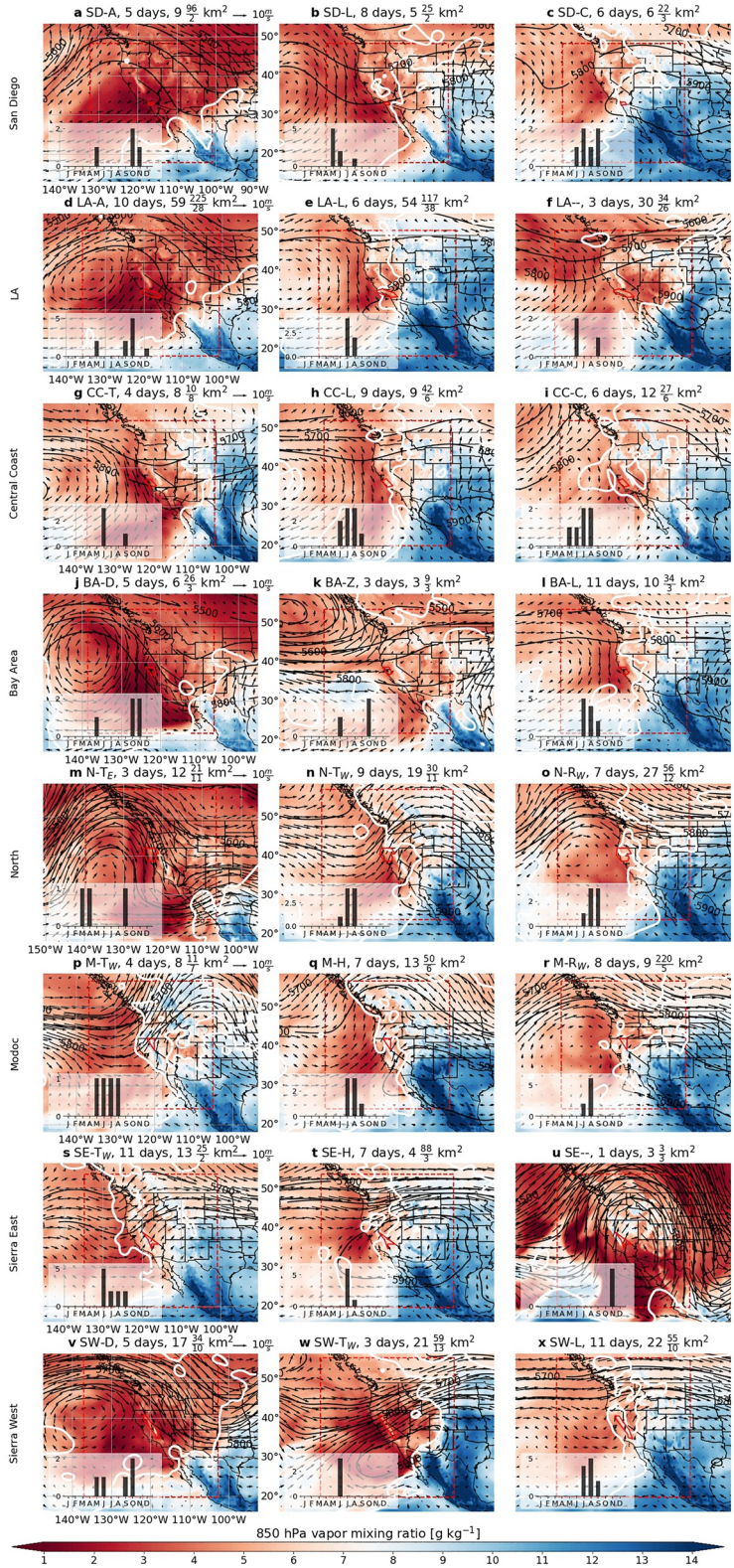

Figure 4.

shown in Figure 6. We find large correlation coefficients between the NCD20C and the ERA5 reanalysis products in all regions, which means that similar days are identified as fire WTs independent of the data set used. However, much smaller correlation coefficients are found when comparing the Manhattan distances of ERA5 with ERA20C. The reasons for the larger differences are unclear but it indicates that the NCD20C is a more reliable product for capturing fire WT days in California. The normalized Manhattan distances shown in Figures 6a and 6b have a minimum of $\sigma/2 = 0.34$ (half the standard deviation of a normalized Gaussian distribution). The smaller range in normalized Manhattan distances in the ERA20C data set is due to the coarser grid spacing of this reanalysis.

Next, we used the calculated Manhattan distances to analyze the monthly frequency of fire WTs. Therefore, we select the 41 days with the smallest Manhattan distances in the period 1970–2010 for each WT in each region. This corresponds to the annual event (i.e., 41 events in a 41 yr long period). Using different return periods such as the one in two or one in 5 yr event leads to similar results (not shown).

Figure 7 shows a comparison of monthly WT frequencies in the NCD20C, ERA20C, and LENS data. The histograms from ERA5 (Figure 4) and NCD20C agree well considering the much smaller sample size of the ERA5 histograms. Also, the current climate NCD20C and ERA20C agree well to each other with the exception of Central Coast Trough (Figure 7f), Bay Area Zonal pattern (Figure 7j), and Sierra West Diablo events (Figure 7t).

Concerning the comparison of LENS and reanalysis data, it is important to note that some differences might not be due to model deficiencies but due to natural climate variability. Generally, LENS can capture the seasonal cycle of most WTs. Larger differences occur in the Northern region's pattern with the ridge in the west, which peaks in August instead of July (Figure 7n). For the other regions and WTs, the differences between LENS and the reanalysis data sets are similarly large compared to the differences between the ERA20C and NCD20C reanalysis.

3.3. Historic and Future Changes of California Fire Weather Patterns

Figure 7 also shows how the ensemble mean LENS monthly frequency of WTs is projected to change by the end of the 21st century (2060–2100). One of the most systematic changes is a significant increase in thermal low WTs in the San Diego (Figure 7b), Los Angeles (Figure 7e), Central Coast (Figure 7g), Bay Area (Figure 7k), and Sierra West (Figure 7b) regions. We will investigate the potential causes of these increases later in this section. Furthermore, systematic decreases occur for the Santa Ana and Diablo WTs (except in the Bay Area), which is in line with previous research (Brewer & Mass, 2016; Guzman-Morales & Gershunov, 2019). We see mixed changes in the response of WTs associated with troughs in the west (T_W). These types increase significantly in the Modoc and Sierra East region but decrease substantially in the Sierra West and Northern region. High-pressure WTs increase in the Modoc and Sierra East region and convective patterns increase in the Central Coast but decrease in San Diego. The seasonality of the WTs stays mostly unchanged except for the troughs in the west patterns (T_W) in the Modoc and Sierra East region that show a shift from mid-summer to late spring and early summer.

Next, we assess changes in the frequency of WTs by selecting the annual event (i.e., the 116 days with the lowest Manhattan distance in the NCD20C record of 1900–2015) and count their frequency in a moving 41 yr long period. Other return periods like the one in 5 yr event lead to similar results (not shown). Performing this analysis on the NCD20C and ERA20C data allows us to calculate "observed" historic changes in WT frequencies. However, trend estimates from reanalysis data sets have to be interpreted with caution since they can be affected by inhomogeneities and artificial signals (Wohland et al., 2019). LENS provides information on the role of natural variability and forced climate change in the observed and projected frequency changes, and SFE allows us to attribute these changes to greenhouse gases or aerosol forcings.

Figure 4. (Previous page.) Fire weather type (WTs) centroids for the San Diego (SD), Los Angeles (LA), Central Coast (CC), Bay Area (BA), North (N) Modoc (M), Sierra East (SE), and Sierra West (SW) region (top-down). The WT average 850 hPa water vapor mixing ratio is shown in filled contours, and the average 500 hPa geopotential height is shown with black contour lines. Additionally, the 850 hPa wind speed and direction are shown with arrows except for the Modoc, Northeast, Sierra East, and Sierra West regions for which the 500 hPa wind field is shown. Histograms in the bottom left show the monthly occurrence frequency of the WT days. The title of each plot shows the number of days in each WT and the median, maximum (numerator), minimum (denominator) burned area, and the WT's acronym. These acronyms are Diablo (D), Santa Ana (A), Trough East (T_E), Trough West (T_W), Ridge (R), Ridge West (R_W), Thermal Low (L), High Pressure (H), Convective (C), Zonal Flow (Z), and none (−).

Journal of Geophysical Research: Atmospheres
10.1029/2021JD035350

Table 2
Summary of the Date, Burned Area (in km^2), and Associated WT for the 19 Days With Largest Burned Area in Each Region That Were Used in the Cluster Analysis

San Diego			Los Angeles			Central Coast			Bay Area			Northern			Modoc			Sierra East			Sierra West		
Date	Area	WT	Date	Area	WT	Date	Area	WT	Date	Area	WT	Date	Area	WT	Date	Area	WT	Date	Area	WT	Date	Area	WT
2007-10-22	96.7	A	2003-10-26	225.6	A	2011-06-19	10.5	T	2017-10-09	26.6	D	2006-09-22	21.6	T_E	2001-05-28	11.7	T_W	2006-09-15	26.0	T_W	2001-09-07	34.6	D
2003-10-26	48.6	A	2017-12-05	224.8	A	2014-06-22	9.3	T	2008-05-22	6.7	D	2010-03-18	12.9	T_E	2002-07-14	8.7	T_W	2006-06-12	24.1	T_W	2017-10-09	32.4	D
2001-01-04	9.8	A	2013-05-03	96.1	A	2016-09-04	8.3	T	2018-10-07	6.2	D	2006-04-27	11.6	T_E	2008-08-18	7.5	T_W	2011-09-14	21.3	T_W	2013-05-02	17.2	D
2014-05-15	9.2	A	2014-05-16	63.9	A	2005-06-05	8.1	T	2011-11-30	4.0	D	2015-08-10	30.3	T_W	2006-06-28	7.4	T_W	2002-07-13	19.2	T_W	2004-10-14	12.7	D
2003-11-05	2.5	A	2007-10-22	62.1	A	2017-07-10	42.4	L	2018-11-10	3.4	D	2004-08-12	23.9	T_W	2001-08-12	50.9	H	2005-08-12	16.4	T_W	2008-06-13	10.6	D
2002-08-03	25.1	L	2006-09-17	57.7	A	2005-08-24	17.4	L	2013-06-24	9.0	Z	2008-06-24	20.7	T_W	2010-07-28	18.6	H	2006-06-27	13.9	T_W	2016-06-25	59.7	T_W
2012-05-25	22.6	L	2005-09-29	43.2	A	2016-09-19	13.5	L	2010-10-23	3.4	Z	2009-08-05	20.1	T_W	2014-08-01	16.4	H	2016-08-05	8.5	T_W	2015-06-21	21.5	T_W
2017-05-20	7.0	L	2006-10-27	36.1	A	2008-06-22	11.5	L	2017-10-18	3.3	Z	2012-08-20	19.9	T_W	2018-07-29	13.6	H	2004-06-26	6.3	T_W	2007-06-24	13.9	T_W
2013-05-24	6.8	L	2008-10-13	32.0	A	2016-07-02	9.3	L	2003-08-28	34.8	L	2018-07-30	16.7	T_W	2012-09-07	12.6	H	2002-06-20	4.9	T_W	2015-09-13	55.8	L
2002-06-20	5.0	L	2001-10-12	28.7	A	2006-08-04	7.4	L	2015-07-23	22.8	L	2012-07-09	13.9	T_W	2004-07-24	6.9	H	2010-07-27	3.0	T_W	2002-07-22	48.8	L
2012-06-18	3.4	L	2016-08-17	117.2	L	2006-07-11	6.8	L	2007-09-07	22.3	L	2014-07-02	13.6	T_W	2017-08-11	6.1	H	2016-06-02	2.4	T_W	2012-08-12	34.5	L
2012-05-17	3.3	L	2013-07-17	80.5	L	2018-06-04	6.6	L	2014-07-05	13.1	L	2008-07-23	11.5	T_W	2012-08-14	220.3	R_W	2007-07-07	88.1	H	2017-07-19	29.6	L
2013-05-07	2.0	L	2016-07-23	56.0	L	2017-08-25	6.2	L	2016-08-03	11.8	L	2014-08-04	56.7	R_W	2017-08-02	49.3	R_W	2006-07-25	10.0	H	2008-07-10	26.5	L
2006-07-29	22.3	C	2013-08-08	52.5	L	2009-08-28	27.5	C	2013-09-09	10.2	L	2008-07-11	29.3	R_W	2003-07-21	12.7	R_W	2005-07-20	7.6	H	2011-09-11	22.4	L
2016-06-21	8.6	C	2004-07-21	44.1	L	2017-05-19	18.9	C	2018-07-03	9.3	L	2004-09-05	28.9	R_W	2006-08-12	10.9	R_W	2015-08-16	4.5	H	2001-08-21	21.1	L
2004-07-14	6.5	C	2017-07-10	38.2	L	2006-07-23	16.4	C	2003-07-21	8.0	L	2001-08-09	27.2	R_W	2015-08-01	7.7	R_W	2002-07-01	4.2	H	2017-07-09	16.6	L
2007-09-13	5.6	C	2016-09-19	34.2		2018-08-07	9.5	C	2015-08-20	7.2	L	2017-09-03	20.7	R_W	2005-08-25	7.5	R_W	2009-07-19	3.6	H	2014-08-19	13.5	L
2012-08-16	4.4	C	2002-06-06	30.9		2012-07-09	6.6	C	2009-08-13	4.8	L	2018-08-26	14.0	R_W	2018-07-14	5.7	R_W	2018-07-10	3.6	H	2013-08-24	10.8	L
2010-09-03	3.0	C	2016-06-17	26.2		2016-06-05	6.6	C	2006-07-01	3.8	L	2013-09-10	12.7	R_W	2018-08-20	5.4	R_W	2002-11-21	3.2		2016-08-20	10.3	L

Note. The identified WT are: Diablo (D), Santa Ana (A), Trough East (T_E), Trough West (T_W), Ridge (R), Ridge West (R_W), Thermal Low (L), High Pressure (H), Convective (C), and none (−) for days with small burned areas that were outliers in the cluster analysis (i.e., are dissimilar to the identified WTs).

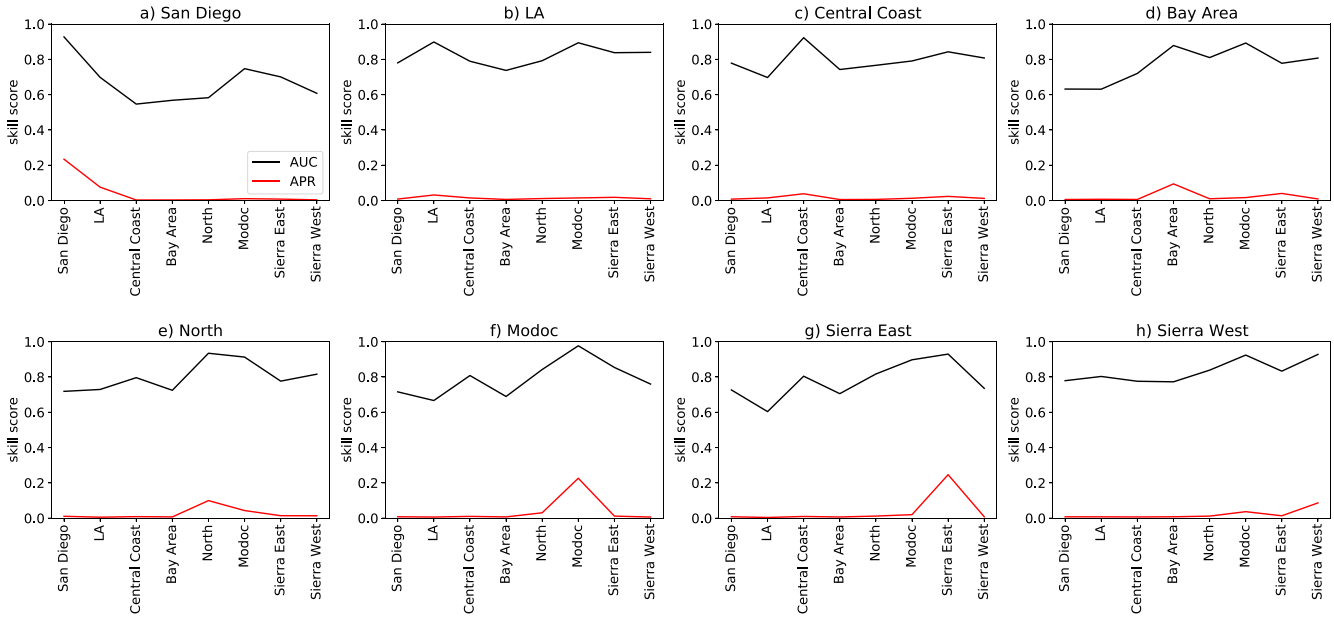

Figure 5. Area under the ROC curve (AUC; black lines) and Average Precision-Recall score (APR, red lines) when using the WT centroids from one region to identify large fire growth days in the other regions.

Time series of the annual average changes in WTs from the NCD20C, ERA20C, LENS, and SFR are shown in Figure 8. Comparing historic changes in WT frequencies shows that the observed changes can differ largely between the NCD20C and the ERA20C analysis in some regions and WTs and, additionally, these changes can be different than the simulated changes such as for the occurrence of Diablo and Santa Ana events. Diablo and Santa Ana events show an increasing frequency in the reanalysis (except for the Sierra West region in ERA20C) but no change or slight decreases in the LENS data. These differences can have two reasons: first, the model is unable to simulate historic climate trends, and/or second, the historic trend was predominantly caused by natural climate variability and does not correspond to the forced change that is represented by the LENS ensemble mean. The significant variability in the historic NCD20C and ERA20C reanalysis WT changes suggests that long-term natural climate variability is large and can dominate the change signal.

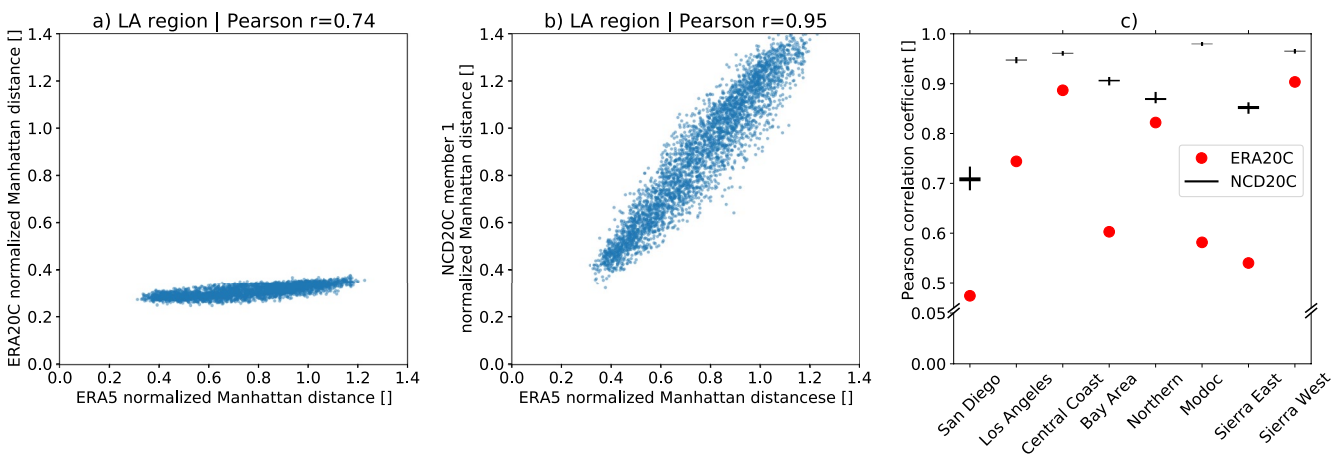

Figure 6. Comparison of daily minimum (over WTs) normalized Manhattan distances between ERA5 and ERA20C (a) and ERA5 and NCD20C (b) within the period 2001–2010 in the LA region. Shown are Manhattan distances that are normalized according to the number of grid cells and variables in each data set. Pearson correlation coefficient of daily minimum Manhattan distances between ERA20C against ERA5 (red dot) and the 80-member ensemble NCD20C distances against ERA5 (box-whisker plots) are shown for each region in panel (c). The box shows the ensemble interquartile range and the whiskers show the minimum and maximum correlation coefficient in the NCD20C ensemble.

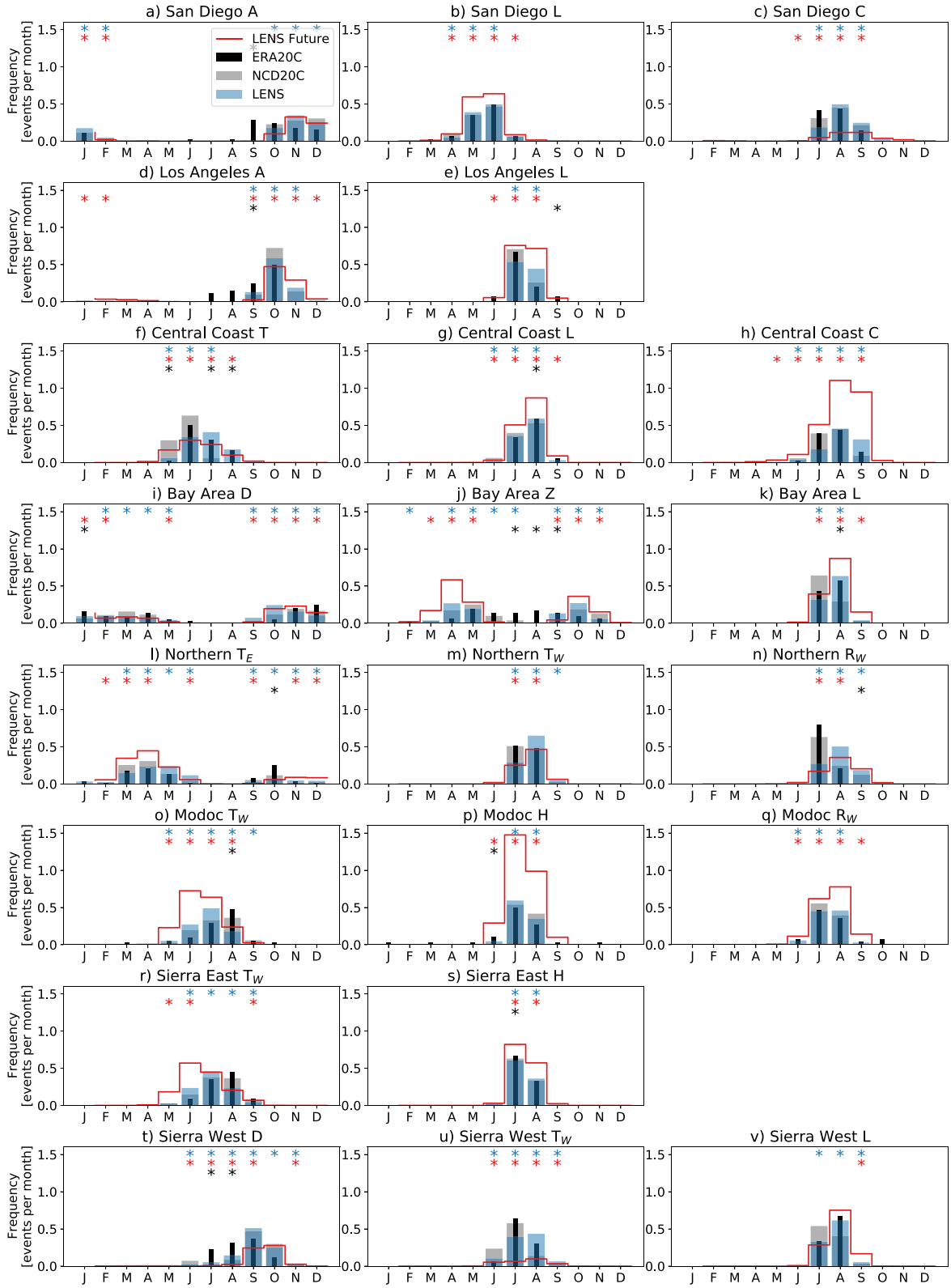

Figure 7.

Comparing the LENS with the SFR time series in Figure 8 allows us to understand the forcing that causes WT frequency changes. For most WTs, the ensemble mean frequencies in the LENS and the SFR are similar throughout the 20th century indicating that forced climate change was within the bounds of natural variability in the past. This changes for many WT patterns in the future. In Figure 7, we already identified an increase in thermal low patterns, which in the San Diego and Los Angeles region (Figures 8b and 8e) is mainly caused by greenhouse gas increases but largely results from changes in the aerosol concentrations in other regions. The decreases in Diablo and Santa Ana WT events are related to greenhouse gas emissions. The two regions that might be most affected by WT frequency changes are the Modoc and Sierra East. All of the WTs in these regions show significant increase mainly due to increased greenhouse gases.

One of the main outcomes of this analysis is the systematic increase of thermal low-pressure system WTs that might be a leading contributor to future periods during which weather can support large daily fire growth in California. To better understand the reason for the increasing frequency in thermal low-pressure systems, we must first understand under which conditions they form. Figure 9 shows the daily maximum temperature, relative humidity, 500 hPa geopotential height, and 850 hPa wind field anomalies during the six Los Angeles thermal Low WT days that occurred within the daily burned area observational record (see Table 2). Anomalies are calculated compared to the average July and August conditions, which are the peak months of these WTs. Much of the area within the Los Angeles region and its surroundings show significantly warmer temperatures and lower relative humidity. There are no significant anomalies in the geopotential height field in the weather typing domain but the 850 hPa field shows anomalously strong onshore flow into the Los Angeles region. The differential heating of the land compared to the ocean causes the heated air to rise over land and results in divergence flow aloft, which creates the thermal low. In addition to the very dry and hot conditions, fire risk is further enhanced by the presence of CAPE (Figure 4e), which makes these environments conductive to plume-driven fires. Climate change will further increase the ocean-land temperature gradient in July and August while relative humidity is projected to stay similar (Figure 10). This increase in differential heating is more favorable for the development of thermal low-pressure systems.

Changes in the aerosol forcing also affect the frequency of thermal lows, particularly in northern and central California where aerosol changes can dominate the change signal (e.g., in the Bay Area, Figure 8k). Figure 11 shows that keeping greenhouse gas concentrations constant results in significantly reduced sea level pressure along the coast of California in addition to significantly reduced relative humidity during July and August. These changes are a combination of changes in aerosol forcing, land use/land cover, stratospheric and tropospheric ozone, and natural radiative forcings. We hypothesize that this decrease in sea level pressure is enhancing the frequency of thermal lows pressure systems, however, the decrease might very well be related to more frequent thermal lows. Additionally, the reduction in relative humidity over land is likely to increase sensible heating, which in turn is favorable for the development of thermal lows. A more detailed analysis of how changes in aerosol forcing could cause a decrease in coastal sea level pressure and relative humidity is beyond the scope of this study but should be the focus of future research.

As seen in Figure 8k, the large increase in projected thermal low-pressure WT frequencies in the 21st century is a combination of the changes in greenhouse-gas and aerosol forcing where greenhouse-gas forcing is more important in San Diego and Los Angeles and aerosol forcing changes are more important in the central and northern regions.

We do not perform an in-depth analysis of the causes of decreasing Santa Ana and Diabolo events since previous studies have already shown that climate change decreases the southwestward pressure gradient force that drives these winds (Guzman-Morales & Gershunov, 2019).

Figure 7. Monthly frequency of current climate (1970–2010) WTs in the NCD20C (gray bars), ERA20C (black bars), LENS (blue bars), and future climate (2060–2100) LENS simulations (red line). Results for different fire regions are shown in rows and WTs are shown in columns. Months that have significantly different WT frequencies in the current climate LENS simulations compared to NCD20C are highlighted with a blue asterisk and months where ERA20C frequencies are outside of the NSD20C spread are highlighted with a black star. Months with significant changes in future climate WT frequencies are highlighted with a red asterisk. Significance is assessed by a two-sided Mann-Whitney U test ($P = 0.05$).

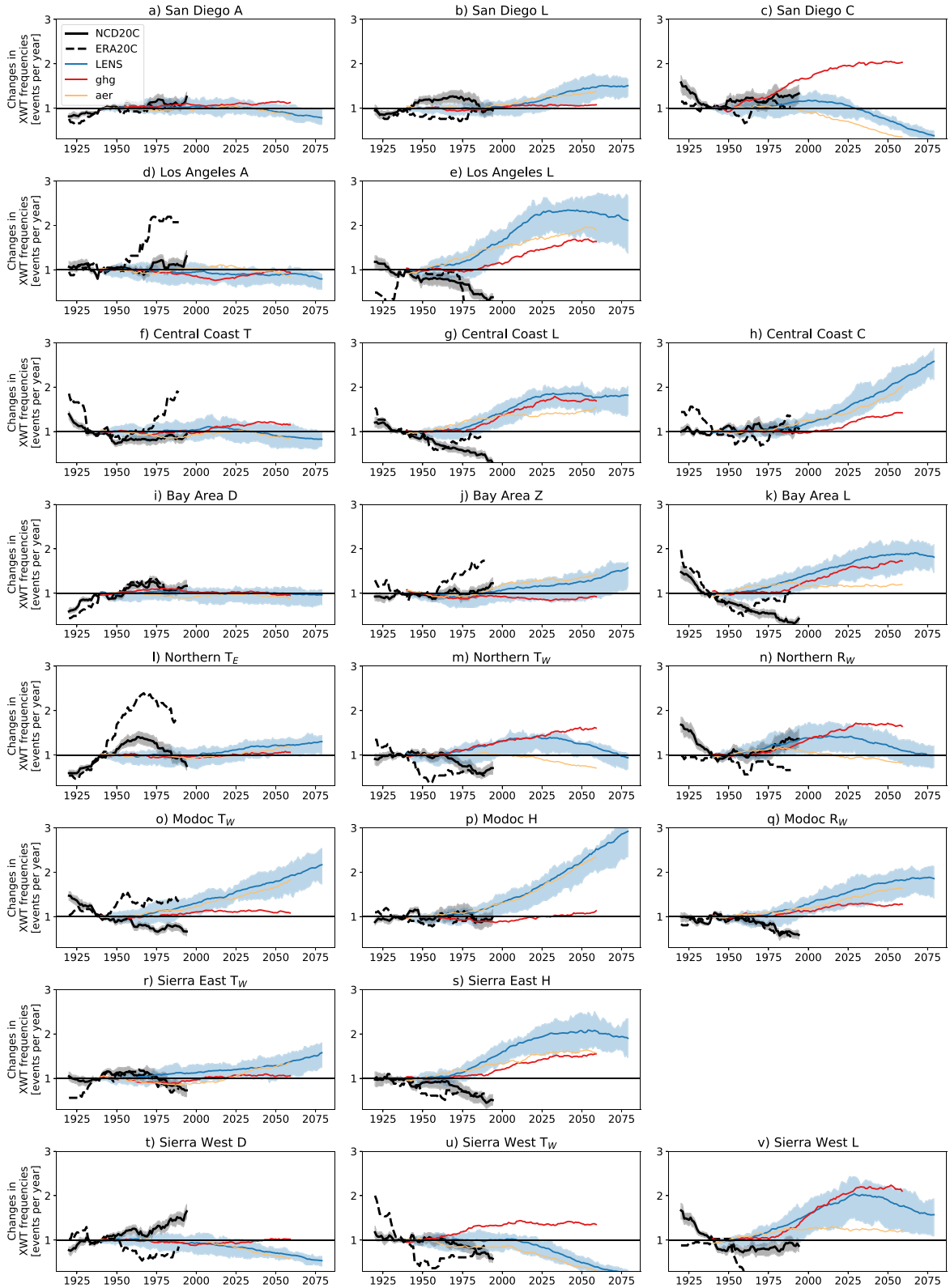

Figure 8. Changes in the 41 yr moving average ensemble mean time series of annual WT frequencies in different fire regions (rows) and for different WTs (columns) relative to the reference period 1920–1960. Results are shown for the NCD20C reanalyses (black solid line), ERA20C (black dashed line), LENS (blue line), no-GHG (red line), and no-AER (orange line). Additionally, the interquartile ensemble spread of the LENS (blue contour) and NCD20C (gray contour) is shown.

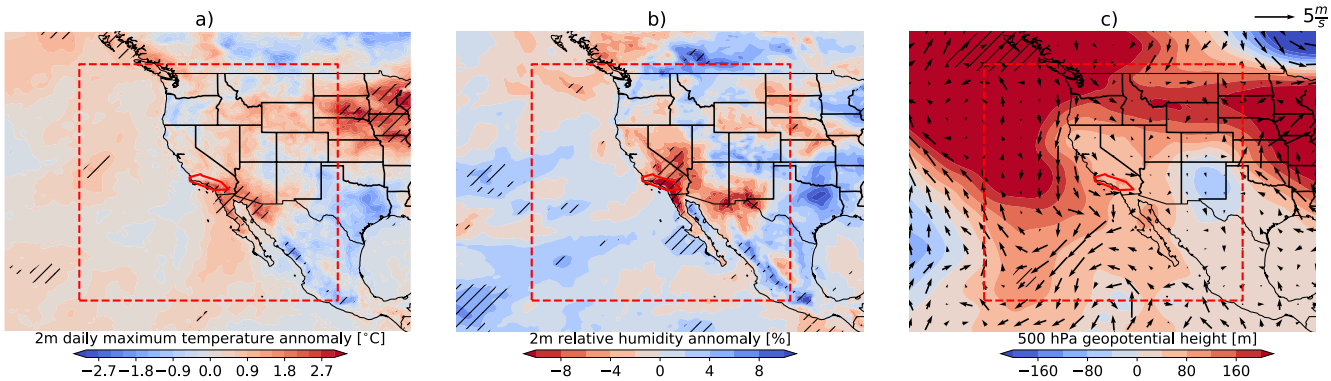

Figure 9. Two meters above ground daily maximum temperature (a), daily average relative humidity (b), 500 hPa height geopotential height (c), and 850 hPa wind field (c) anomalies comparing Los Angeles thermal low WT conditions (6 days in Table 2) with the 2001–2019 July and August mean conditions. Hatching indicates significant anomalies according to the two-sided Mann Whitney U test ($P = 0.05$).

4. Conclusions

We use a clustering approach to identify fire WTs that are related to observed extreme daily burned areas in sub-regions of California. Many of the identified types are similar to fire weather patterns that were identified in the 1960s using a more subjective methodology and different input data (Schroeder et al., 1964). This similarity indicates that these patterns are robust contributors to extreme fires in California. Additionally, the similarity confirm that the Schroeder et al. (1964) patterns, which were based on fire weather not actual burned area, are related to the largest daily burned area days on record. We also found a few additional patterns that were not included in (Schroeder et al., 1964), such as a strong zonal flow pattern in the Bay Area, or an east Pacific ridge pattern that causes large burned areas in the Northern and Modoc region. The reasons why these patterns were not identified in (Schroeder et al., 1964) is unclear but their existence indicates that there might be other so-far undetected patterns that did not occur in our observational record. One major benefit of our results is that we present an objective method that allows to identify potential dangerous fire weather patterns in numerical weather and climate model data, which was not feasible with the results presented in Schroeder et al. (1964).

The main fire WTs and their projected frequency changes by the end of the 21st century are:

1. Diablo and Santa Ana winds: A large pressure gradient between the U.S. desert southwest and California is driving strong, very dry downslope winds. This WT occurs most frequently in fall but has a secondary peak in

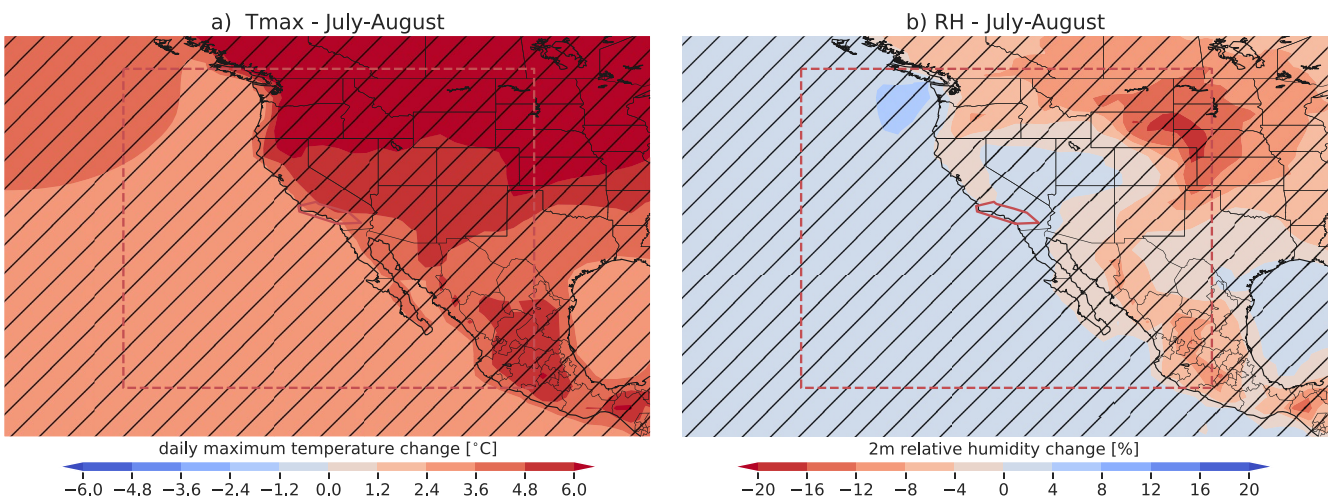

Figure 10. Two meters above ground daily maximum temperature (a) and daily average relative humidity (b) climate change signals from the ensemble mean LENS simulations comparing July and August conditions during 1975–2015 with 2060–2100. Hatching indicates significant anomalies according to the two-sided Mann Whitney U test ($P = 0.05$).

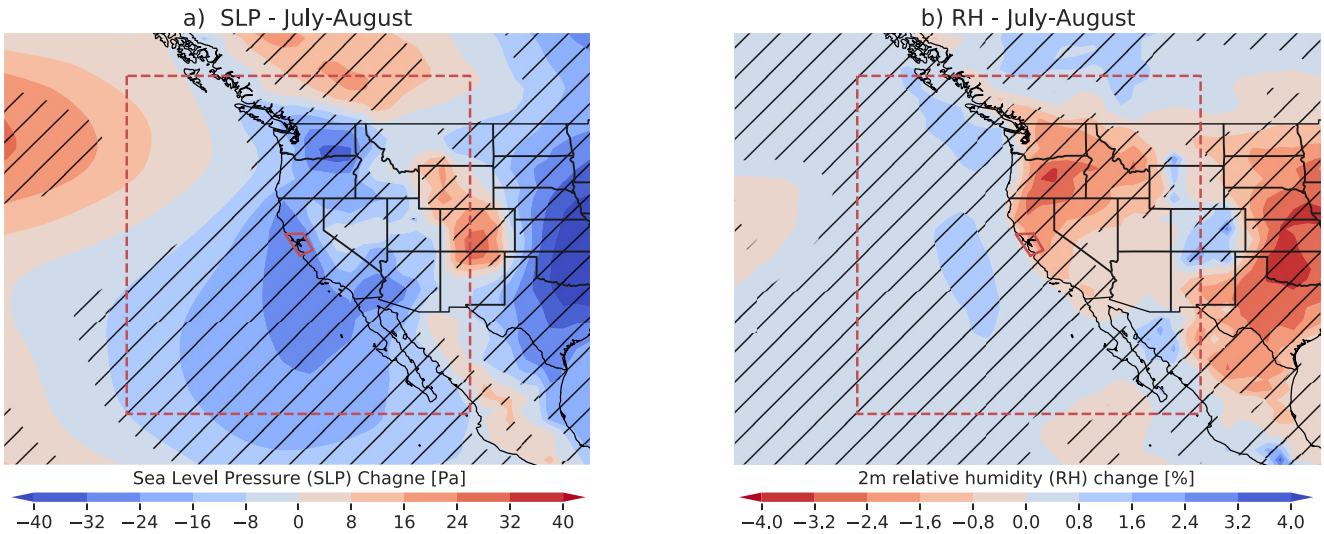

Figure 11. Sea level pressure (a) and daily average relative humidity (b) climate change signals from the ensemble mean SFR simulations without greenhouse-gas concentration increases comparing July and August conditions during 1975–2015 with 2040–2080. Hatching indicates significant anomalies according to the two-sided Mann Whitney U test ($P = 0.05$).

spring. The affected regions are San Diego, Los Angeles, Bay Area, and Sierra West. 20th century reanalyses indicate that Diablo and Santa Ana events increased in frequency during the last century. This trend is not expected to continue since climate model projections show that these events decrease in frequency (except in the Bay area) as a result of increasing greenhouse gas forcing, which is in line with previous research (Guzman-Morales & Gershunov, 2019)

2. Thermal low-pressure systems: The differential heating over land compared to the east Pacific during the peak of summer results in the development of shallow low-pressure systems in California (thermal lows). Thermal low WTs are associated with anomalously dry and hot conditions over land and can partly feature atmospheric instabilities that can support plume-driven fires. Thermal low WTs are projected to become significantly more frequent due to a greenhouse gas-induced increase in the ocean-land temperature gradient and an aerosol forcing-induced low-pressure anomaly over coastal California and drying over land
3. Meridional ridge-southwest (T_W): Anomalously dry and strong southwesterly winds are triggered by a trough in the eastern Pacific that causes large fire growth in central and northern California. This WT occurs typically in summer and early fall and is projected to significantly increase in frequency in the Modoc and Sierra East region but decrease in the North and Sierra West region
4. High pressure: This WT occurs due to a westward shift in the subtropical high causing very hot and dry conditions and rapid fire growth in the Modoc and Sierra East region during summer. High-pressure WTs are expected to increase in frequency in the Modoc due to greenhouse gas forcings and, in the Sierra East region, a combination of greenhouse gas and aerosol change
5. Convective: Atmospheric instability is the dominant feature in this WT that promotes rapid-fire growth in southern California during late summer. This pattern is projected to decrease in San Diego but increase in the Central Coast region

It is important to notice that the presence of a fire WT day is not sufficient for the occurrence of extreme burned areas since fire ignition and suitable fuels and fuel condition also must be present. Previous studies have shown a relationship between the occurrence of strong winds (e.g., Santa Ana winds) and fire ignitions from utility lines (Mitchell, 2013). Future analysis should focus on the relationship between fire WTs and dry lightning. Additionally, fire growth is also modulated by antecedent conditions (Higuera & Abatzoglou, 2020; Holden et al., 2018; Parks & Abatzoglou, 2020; Potter & McEvoy, 2021), which can effects the severity of a fire WT day. Lastly, we emphasize that we derive WTs over a comparatively short period of 20 yr. Thus, there might be additional fire WTs that we did not detect due to the short record and there might be patterns that become extreme under future warmer and drier conditions.

Although some of the WT frequencies have significantly changed during the 20th century, most of these changes are due to climate internal variability. Future analyses should focus on the origins of the historic trends and the origin of the large natural variability in historic time series ideally by using an ensemble of 20th century reanalysis products (Wohland et al., 2019). Additionally, studies could focus on the decadal variations in fire WTs in the future and how those vary among regions. It is also possible that regions in California such as the Central Valley and the Desert Southeast that did not have enough recorded fires to be included in this analysis become more susceptible to fires in the future. How hazardous fire weather patterns look like in these regions could be assets by using for example, a fire weather index rather than fire observations to perform similar analyses as presented here.

We anticipate that future climate change will have a much more pronounced impact on the frequency of fire WTs than past changes. Extreme fire weather in California might be more frequent in future summers and less frequent in fall due to the systematic decrease of Diablo and Santa Ana WTs and the significant increase in thermal low and high-pressure WTs. These changes in WT frequencies will occur on top of other factors such as hotter and drier summers (Lenihan et al., 2003). Importantly, changes in WT frequencies do not solely depend on increasing greenhouse gas concentrations but are a result of the complex interactions between changes in greenhouse gases and aerosols. This means that significant increases in some WTs such as thermal lows in central and northern California might occur even with aggressive greenhouse gas emission reductions.

Data Availability Statement

ERA5 (Hersbach et al., 2020) and ERA20C (Poli et al., 2016) data can be accessed from Copernicus (2022). The NOAA-CIRES-DOE 20th Century Reanalysis V3 (Slivinski et al., 2019) data can be downloaded from NOAA-CIRES-DOE (2022). Fire observations can be accessed as follows: The Global Wildfire Information System (GWIS; Artés et al., 2017) from Artés Vivancos and San-Miguel-Ayanz (2018) and the Monitoring Trends in Burn Severity (MTBS) from USDA (2022). The code for the statistical analysis and visualization of data in this document can be accessed from Prein (2021).

Acknowledgments
NCAR is sponsored by the National Science Foundation. Computer resources were provided by the Computational and Information Systems Laboratory (NCAR Community Computing; http://n2t.net/ark:/85065/d7wd3xhc) This work was sponsored in part by the California Energy Commission—Energy Program Investment Charge (EPIC) program under Grant #EPC-18-026. The authors thank Sean A. Parks for sharing his daily burned area product.

References

Abatzoglou, J. T., & Kolden, C. A. (2011). Relative importance of weather and climate on wildfire growth in interior Alaska. *International Journal of Wildland Fire*, *20*(4), 479–486. https://doi.org/10.1071/wf10046

Abatzoglou, J. T., & Williams, A. P. (2016). Impact of anthropogenic climate change on wildfire across western U.S. forests. *Proceedings of the National Academy of Sciences*, *113*(42), 11770–11775. https://doi.org/10.1073/pnas.1607171113

Aggarwal, C. C., Hinneburg, A., & Keim, D. A. (2001). On the surprising behavior of distance metrics in high dimensional space. In *International Conference on Database Theory* (pp. 420–434). https://doi.org/10.1007/3-540-44503-x_27

Amiro, B. D., Logan, K. A., Wotton, B. M., Flannigan, M. D., Todd, J. B., Stocks, B., & Martell, D. (2005). Fire weather index system components for large fires in the Canadian boreal forest. *International Journal of Wildland Fire*, *13*(4), 391–400.

Artés, T., Cencerrado, A., Cortés, A., & Margalef, T. (2017). Time aware genetic algorithm for forest fire propagation prediction: Exploiting multi-core platforms. *Concurrency and Computation: Practice and Experience*, *29*(9), e3837. https://doi.org/10.1002/cpe.3837

Artés, T., Oom, D., De Rigo, D., Durrant, T. H., Maianti, P., Libertà, G., & San-Miguel-Ayanz, J. (2019). A global wildfire data set for the analysis of fire regimes and fire behavior. *Scientific Data*, *6*(1), 1–11. https://doi.org/10.1038/s41597-019-0312-2

Artés Vivancos, T., & San-Miguel-Ayanz, J. (2018). Global Wildfire Database for GWIS. [Data Set]. . https://doi.org/10.1594/PANGAEA.895835

Balch, J. K., Bradley, B. A., Abatzoglou, J. T., Nagy, R. C., Fusco, E. J., & Mahood, A. L. (2017). Human-started wildfires expand the fire niche across the United States. *Proceedings of the National Academy of Sciences*, *114*(11), 2946–2951. https://doi.org/10.1073/pnas.1617394114

Beals, E. A. (1914). The value of weather forecasts in the problem of protecting forests from fire. *Monthly Weather Review*, *42*(2), 111–119. https://doi.org/10.1175/1520-0493(1914)42<111:tvowfi>2.0.co;2

Bedsworth, L., Cayan, D., Franco, G., Fisher, L., Ziaja, S., & Ackerly, D. D. (2018). *Statewide Summary Report, Californiaâs Fourth Climate Change Assessment. Governor's Office of Planning and Research*. Retrieved from http://climateassessment.ca.gov

Brewer, M. C., & Mass, C. F. (2016). Projected changes in heat extremes and associated synoptic-and mesoscale conditions over the Northwest United States. *Journal of Climate*, *29*(17), 6383–6400. https://doi.org/10.1175/jcli-d-15-0641.1

Buitinck, L., Louppe, G., Blondel, M., Pedregosa, F., Mueller, A., Grisel, O., et al. (2013). API design for machine learning software: Experiences from the scikit-learn project. In *ECML PKDD Workshop: Languages for data mining and machine learning* (pp. 108–122).

Copernicus. (2022). ERA5 hourly data on single levels from 1979 to present. [Data Set]. . https://doi.org/10.24381/cds.adbb2d47

Davies, D., Ederer, G., Olsina, O., Wong, M., Cechini, M., & Boller, R. (2019). *NASA's Fire Information for Resource Management System (FIRMS): Near real-time global fire monitoring using data from MODIS and VIIRS*.

Deser, C., Phillips, A. S., Simpson, I. R., Rosenbloom, N., Coleman, D., Lehner, F., et al. (2020). Isolating the evolving contributions of anthropogenic aerosols and greenhouse gases: A new CESM1 large ensemble community resource. *Journal of Climate*, *33*(18), 7835–7858. https://doi.org/10.1175/jcli-d-20-0123.1

Dong, L., Leung, L. R., Qian, Y., Zou, Y., Song, F., & Chen, X. (2021). Meteorological environments associated with California wildfires and their potential roles in wildfire changes during 1984–2017. *Journal of Geophysical Research: Atmospheres*, *126*(5), e2020JD033180. https://doi.org/10.1029/2020jd033180

Eidenshink, J., Schwind, B., Brewer, K., Zhu, Z.-L., Quayle, B., & Howard, S. (2007). A project for monitoring trends in burn severity. *Fire ecology*, *3*(1), 3–21. https://doi.org/10.4996/fireecology.0301003

FIRE, C. (2020). *Top 20 largest California wildfires*. Retrieved from https://www.fire.ca.gov/media/11416/top20_acres.pdf
Foley, J. C. (1947). *A study of meteorological conditions associated with bush and grass fires and fire protection strategy in Australia*.JJ Gourley, Government Printer.
Fosberg, M. A. (1978). Weather in wildland fire management: The fire weather index. In *Proceedings of the Conference on Sierra Nevada Meteorology, 19–21 June 1978* (pp. 1–4). American Meteorological Society.
Goodrick, S. L. (2002). Modification of the Fosberg fire weather index to include drought. *International Journal of Wildland Fire*, *11*(4), 205–211. https://doi.org/10.1071/wf02005
Guzman-Morales, J., & Gershunov, A. (2019). Climate change suppresses Santa Ana winds of Southern California and sharpens their seasonality. *Geophysical Research Letters*, *46*(5), 2772–2780.
Guzman-Morales, J., Gershunov, A., Theiss, J., Li, H., & Cayan, D. (2016). Santa Ana Winds of Southern California: Their climatology, extremes, and behavior spanning six and a half decades. *Geophysical Research Letters*, *43*(6), 2827–2834.
Haines, D. A. (1989). A lower atmosphere severity index for wildlife fires. *National Weather Digest*, *13*, 23–27.
Hammer, R. B., Radeloff, V. C., Fried, J. S., & Stewart, S. I. (2007). Wildland-urban interface housing growth during the 1990s in California, Oregon, and Washington. *International Journal of Wildland Fire*, *16*(3), 255–265. https://doi.org/10.1071/wf05077
Hersbach, H., Bell, B., Berrisford, P., Hirahara, S., Horányi, A., Muñoz-Sabater, J., et al. (2020). The ERA5 global reanalysis. *Quarterly Journal of the Royal Meteorological Society*, *146*(730), 1999–2049. https://doi.org/10.1002/qj.3803
Higuera, P. E., & Abatzoglou, J. T. (2020). Record-setting climate enabled the extraordinary 2020 fire season in the western United States. *Global Change Biology*, *27*, 1–2.
Holden, Z. A., Swanson, A., Luce, C. H., Jolly, W. M., Maneta, M., Oyler, J. W., & Affleck, D. (2018). Decreasing fire season precipitation increased recent western U.S. forest wildfire activity. *Proceedings of the National Academy of Sciences*, *115*(36), E8349–E8357. https://doi.org/10.1073/pnas.1802316115
Huang, C., Lin, Y. L., Kaplan, M., & Charney, J. (2009). Synoptic-scale and mesoscale environments conducive to forest fires during the October 2003 extreme fire event in Southern California. *Journal of Applied Meteorology and Climatology*, *48*(3), 553–579. https://doi.org/10.1175/2008jamc1818.1
Hull, M. K., O'Dell, C. A., & Schroeder, M. J. (1966). Critical fire weather patterns, their frequency and levels of fire danger (*Tech. Rep.)*. Berkeley CA: Pacific Southwest Forest and Range Experiment Station. https://doi.org/10.21236/ad0634565
Jin, Y., Goulden, M. L., Faivre, N., Veraverbeke, S., Sun, F., Hall, A., et al. (2015). Identification of two distinct fire regimes in Southern California: Implications for economic impact and future change. *Environmental Research Letters*, *10*(9), 094005. https://doi.org/10.1088/1748-9326/10/9/094005
Jin, Y., Randerson, J. T., Faivre, N., Capps, S., Hall, A., & Goulden, M. L. (2014). Contrasting controls on wildland fires in Southern California during periods with and without Santa Ana winds. *Journal of Geophysical Research: Biogeosciences*, *119*(3), 432–450. https://doi.org/10.1002/2013jg002541
Jolly, W. M., Cochrane, M. A., Freeborn, P. H., Holden, Z. A., Brown, T. J., Williamson, G. J., & Bowman, D. M. (2015). Climate-induced variations in global wildfire danger from 1979 to 2013. *Nature Communications*, *6*(1), 1–11. https://doi.org/10.1038/ncomms8537
Joy, G. C. (1923). Forest fire weather in western Washington. *Monthly Weather Review*, *51*(11), 564–566. https://doi.org/10.1175/1520-0493(1923)51<564:ffwiww>2.0.co;2
Kay, J. E., Deser, C., Phillips, A., Mai, A., Hannay, C., Strand, G., et al. (2015). The Community Earth System Model (CESM) large ensemble project: A community resource for studying climate change in the presence of internal climate variability. *Bulletin of the American Meteorological Society*, *96*(8), 1333–1349. https://doi.org/10.1175/bams-d-13-00255.1
Lamarque, J. F., Kyle, G. P., Meinshausen, M., Riahi, K., Smith, S. J., van Vuuren, D. P., et al. (2011). Global and regional evolution of short-lived radiatively-active gases and aerosols in the Representative Concentration Pathways. *Climatic Change*, *109*, 191. https://doi.org/10.1007/s10584-011-0155-0
Lenihan, J. M., Drapek, R., Bachelet, D., & Neilson, R. P. (2003). Climate change effects on vegetation distribution, carbon, and fire in California. *Ecological Applications*, *13*(6), 1667–1681. https://doi.org/10.1890/025295
McCarthy, E. F. (1923). Forest fire weather in the southern Appalachians. *Monthly Weather Review*, *51*(4), 182–185. https://doi.org/10.1175/1520-0493(1923)51<182:ffwits>2.0.co;2
McInnes, L., Healy, J., & Astels, S. (2017). hdbscan: Hierarchical density based clustering. *Journal of Open Source Software*, *2*(11), 205. https://doi.org/10.21105/joss.00205
Meinshausen, M., Smith, S. J., Calvin, K., Daniel, J. S., Kainuma, M. L. T., Lamarque, J.-F., et al. (2011). The RCP greenhouse gas concentrations and their extensions from 1765 to 2300. *Climatic Change*, *109*, 213. https://doi.org/10.1007/s10584-011-0156-z
Mitchell, J. W. (2013). Power line failures and catastrophic wildfires under extreme weather conditions. *Engineering Failure Analysis*, *35*, 726–735. https://doi.org/10.1016/j.engfailanal.2013.07.006
Munich-Re. (2019). *New hazard and risk level for wildfires in California and worldwide*. Retrieved from https://doi.org/10.1016/j.landusepol.2021.105502
Newark, M. (1975). The relationship between forest fire occurrence and 500 mb longwave ridging. *Atmosphere*, *13*(1), 26–33. https://doi.org/10.1080/00046973.1975.9648385
Nimchuk, N. (1983). Wildfire behavior associated with upper ridge breakdown. ENR Rep. no. T/50. Alberta Energy and Natural Resources. Forestry Service.
NOAA-CIRES-DOE. (2022). NOAA-CIRES-DOE 21th Century Reanalysis (V3). [Data Set]. . Retrieved from https://psl.noaa.gov/data/20thC_Rean/
Parks, S. A., & Abatzoglou, J. (2020). Warmer and drier fire seasons contribute to increases in area burned at high severity in western U.S. forests from 1985 to 2017. *Geophysical Research Letters*, *47*(22), e2020GL089858. https://doi.org/10.1029/2020gl089858
Parks, S. A., Miller, C., Parisien, M.-A., Holsinger, L. M., Dobrowski, S. Z., & Abatzoglou, J. (2015). Wildland fire deficit and surplus in the western United States, 1984–2012. *Ecosphere*, *6*(12), 1–13. https://doi.org/10.1890/es15-00294.1
Pedregosa, F., Varoquaux, G., Gramfort, A., Michel, V., Thirion, B., Grisel, O., et al. (2011). Scikit-learn: Machine learning in Python. *Journal of Machine Learning Research*, *12*, 2825–2830.
Peterson, D. A., Hyer, E. J., Campbell, J. R., Fromm, M. D., Hair, J. W., Butler, C. F., & Fenn, M. A. (2015). The 2013 Rim Fire: Implications for predicting extreme fire spread, pyroconvection, and smoke emissions. *Bulletin of the American Meteorological Society*, *96*(2), 229–247. https://doi.org/10.1175/bams-d-14-00060.1
Poli, P., Hersbach, H., Dee, D. P., Berrisford, P., Simmons, A. J., Vitart, F., et al. (2016). ERA-20C: An atmospheric reanalysis of the 21th century. *Journal of Climate*, *29*(11), 4083–4097. https://doi.org/10.1175/jcli-d-15-0556.1

Potter, B. E. (2012a). Atmospheric interactions with wildland fire behavior—I. Basic surface interactions, vertical profiles and synoptic structures. *International Journal of Wildland Fire*, *21*(7), 779–801. https://doi.org/10.1071/wf11128

Potter, B. E. (2012b). Atmospheric interactions with wildland fire behavior—II. Plume and vortex dynamics. *International Journal of Wildland Fire*, *21*(7), 802–817. https://doi.org/10.1071/wf11129

Potter, B. E., & McEvoy, D. (2021). Weather factors associated with extremely large fires and fire growth days. *Earth Interactions*, *25*(1), 160–176. https://doi.org/10.1175/ei-d-21-0008.1

Prein, A. F. (2021). California-extreme-fire-weather-types. [Software]. . Retrieved from https://github.com/AndreasPrein/California-extreme-fire-weather-types. https://doi.org/10.5281/zenodo.1234

Prein, A. F., Holland, G. J., Rasmussen, R. M., Clark, M. P., & Tye, M. R. (2016). Running dry: The U.S. Southwest's drift into a drier climate state. *Geophysical Research Letters*, *43*(3), 1272–1279. https://doi.org/10.1002/2015gl066727

Prein, A. F., & Mearns, L. O. (2021). U.S. extreme precipitation weather types increased in frequency during the 20th century. *Journal of Geophysical Research: Atmospheres*, *16*, e2020JD034287. https://doi.org/10.1029/2020jd034287

Radeloff, V. C., Helmers, D. P., Kramer, H. A., Mockrin, M. H., Alexandre, P. M., Bar-Massada, A., et al. (2018). Rapid growth of the U.S. wildland-urban interface raises wildfire risk. *Proceedings of the National Academy of Sciences*, *115*(13), 3314–3319. https://doi.org/10.1073/pnas.1718850115

Riley, K. L., Abatzoglou, J. T., Grenfell, I. C., Klene, A. E., & Heinsch, F. A. (2013). The relationship of large fire occurrence with drought and fire danger indices in the western USA, 1984–2008: The role of temporal scale. *International Journal of Wildland Fire*, *22*(7), 894–909. https://doi.org/10.1071/wf12149

Saito, T., & Rehmsmeier, M. (2015). The precision-recall plot is more informative than the ROC plot when evaluating binary classifiers on imbalanced data sets. *PLoS One*, *10*(3). https://doi.org/10.1371/journal.pone.0118432

Schiemann, R., & Frei, C. (2010). How to quantify the resolution of surface climate by circulation types: An example for Alpine precipitation. *Physics and Chemistry of the Earth, Parts A/B/C*, *35*(9–12), 403–410. https://doi.org/10.1016/j.pce.2009.09.005

Schroeder, M. J., Glovinsky, M., Henricks, V. F., Hood, F. C., & Hull, M. K. (1964). *Synoptic weather types associated with critical fire weather (Tech. Rep.)*. Berkeley CA: Pacific Southwest Forest and Range Experiment Station.

Slivinski, L. C., Compo, G. P., Whitaker, J. S., Sardeshmukh, P. D., Giese, B. S., McColl, C., et al. (2019). Towards a more reliable historical reanalysis: Improvements for version 3 of the 21th Century Reanalysis system. *Quarterly Journal of the Royal Meteorological Society*, *145*(724), 2876–2908. https://doi.org/10.1002/qj.3598

Smith, C., Hatchett, B., & Kaplan, M. (2018). *Characteristics of Diablo-like wind conditions in Northern California based on a climatology from surface observations*.

Srock, A. F., Charney, J. J., Potter, B. E., & Goodrick, S. L. (2018). The hot-dry-windy index: A new fire weather index. *Atmosphere*, *9*(7), 279. https://doi.org/10.3390/atmos9070279

Tempel, D. J., Gutierrez, R. J., Whitmore, S. A., Reetz, M. J., Stoelting, R. E., Berigan, W. J., et al. (2014). Effects of forest management on California spotted owls: Implications for reducing wildfire risk in fire-prone forests. *Ecological Applications*, *24*(8), 2089–2106. https://doi.org/10.1890/13-2192.1

USDA. (2022). Monitoring Trends in Burn Severity. [Data Set]. . Retrieved from http://mtbs.gov/

Van Wagner, C. (1974). *Structure of the Canadian forest fire weather ndex* (Vol. 1333). Environment Canada, Forestry Service Ontario.

Verisk. (2020). *Wildfire risk analysis*. Retrieved from https://www.verisk.com/insurance/campaigns/location-fireline-state-risk-report/

Westerling, A. L. (2016). Increasing western U.S. forest wildfire activity: Sensitivity to changes in the timing of spring. *Philosophical Transactions of the Royal Society B: Biological Sciences*, *371*(1696), 20150178. https://doi.org/10.1098/rstb.2015.0178

Wilks, D. S. (2011). *Statistical methods in the atmospheric sciences* (Vol. 100). Academic Press.

Williams, A. P., Abatzoglou, J. T., Gershunov, A., Guzman-Morales, J., Bishop, D. A., Balch, J. K., & Lettenmaier, D. P. (2019). Observed impacts of anthropogenic climate change on wildfire in California. *Earth's Future*, *7*(8), 892–910. https://doi.org/10.1029/2019ef001210

Wohland, J., Omrani, N.-E., Witthaut, D., & Keenlyside, N. S. (2019). Inconsistent wind speed trends in current 20th century reanalyses. *Journal of Geophysical Research: Atmospheres*, *124*(4), 1931–1940. https://doi.org/10.1029/2018jd030083